# Increased Cerebral Iron Uptake in Wilson's Disease: A $^{52}$Fe-Citrate PET Study

Matthias Bruehlmeier, Klaus L. Leenders, Peter Vontobel, Claudio Calonder, Angelo Antonini, and Adolf Weindl

*PET Program, Paul Scherrer Institute, Villigen, Switzerland; and Department of Neurology, Technische Universität Munich, Munich, Germany*

Toxicity of abundant copper is the main cause of brain and liver tissue damage in patients with Wilson's disease (WD). However, there is also evidence of a disturbed iron metabolism in this genetically determined disorder. This PET study was undertaken to assess cerebral iron metabolism in WD patients. **Methods:** We used $^{52}$Fe-citrate, which converts to $^{52}$Fe-transferrin in blood plasma, to study basic pharmacokinetic features of the cerebral iron transport in 6 WD patients and in 16 healthy volunteers (control subjects). A 2-tissue-compartment model and multiple time graphic plotting were used to calculate $^{52}$Fe-transferrin distribution volumes and transport rates. **Results:** Net iron uptake (Ki) from plasma into brain tissue was significantly ($P <$ 0.001) higher in WD patients (Ki [mean ± SEM] = 15.1E-05 ± 7.13E-05 [1/min]) than in healthy volunteers (Ki = 2.66E-05 ± 0.351E-05 [1/min]). There was no difference of tracer iron distribution in the cerebral plasma volume between patients and healthy volunteers. Iron uptake values resulting from 2 methods to model PET data of patients and healthy volunteers were highly correlated ($P < 0.001$). **Conclusion:** An abnormally increased cerebral $^{52}$Fe-transferrin uptake was found in WD patients.

**Key Words:** $^{52}$Fe; iron; brain; PET; Wilson's disease

**J Nucl Med 2000; 41:781–787**

Wilson's disease (WD) is an autosomal recessive disorder resulting in a decreased copper excretion into the bile. Consequently, toxic copper accumulation in the liver and the brain leads to hepatic, neurologic, and psychiatric symptoms (*1,2*). Ceruloplasmin (Cp) is a copper-containing 132-kDa protein with low plasma levels in most WD patients. However, whereas Cp is coded by a gene on chromosome 3 (*3*), the gene coding for WD has been localized on chromosome 13 (*4–6*) and has been cloned (*7,8*). The protein product of the Wilson gene on chromosome 13 is a copper-binding P-type adenosine triphosphatase (designated ATP7B), which plays a role in the incorporation of copper into Cp and in the biliary excretion of copper in the liver.

Cp plays a role in the transmembranous transport of iron (*9,10*). Hereditary Cp deficiency in humans is associated with multiorgan hemosiderosis (*11*). The copper ion of Cp is involved as a redox element in reactions with iron—i.e., Cp catalyzes ferroxidase, which is needed to oxidize the ferrous form of iron ($Fe^{2+}$) to its ferric transport form ($Fe^{3+}$). $Fe^{3+}$ is bound to apotransferrin to form ferrotransferrin as the main transporter protein for iron. In WD, subnormal Cp levels lead to no obvious disturbance of peripheral iron metabolism, but Cp levels below 5% of normal are associated with iron deficiency (*12*).

For these reasons, we suspected a disturbance of iron metabolism in WD patients and addressed this issue by PET. We used $^{52}$Fe-citrate (which converts to $^{52}$Fe-transferrin [Tf] immediately after intravenous administration) to determine basic pharmacokinetic features of the iron uptake in the brains of WD patients and healthy volunteers.

## MATERIALS AND METHODS

### Subjects

We assessed 6 patients suffering from WD (mean age, 36 y; age range, 23–51 y) (Table 1) and compared results with those of 16 healthy volunteers (mean age, 57 y; age range, 37–78 y). WD patients were referred for PET examination by the Department of Neurology, University Hospital of Innsbruck, Innsbruck, Austria (2 patients); Department of Neurology, Cantonal Hospital of Aarau, Aarau, Switzerland (2 patients); Department of Neurology, University Hospital of Munich, Munich, Germany (1 patient); and Department of Neurology, University Hospital of Grosshadern Munich, Munich, Germany (1 patient). For all patients, the diagnosis of WD was based on clinical findings, elevated urinary copper secretion, lowered Cp levels in plasma, and liver biopsy. This study was approved by the local ethical committee of the department of neurology of the University Hospital Zürich. The Swiss Federal Department of Health approved the use of $^{52}$Fe-citrate in humans.

### Properties of $^{52}$Fe

$^{52}Fe^{3+}$-citrate was prepared as described (*13,14*). $^{52}$Fe is a positron emitter, which decays to $^{52m}$Mn with a physical half-life of 8.2 h. $^{52m}$Mn is also a positron emitter, which decays primarily (98.25%) to stable $^{52}$Cr with a half-life of 21 min. PET cannot discriminate the signal of iron from that of manganese in tissue because the sum of the radioactivities of both tracers is measured. This means, that physiologic properties of manganese—for example, transport through the blood–brain barrier (BBB)—may contribute to tissue time–activity curves after $^{52}$Fe-citrate administration. This important point will be discussed because it potentially hampers the validity of $^{52}$Fe-citrate PET results.

Received Mar. 15, 1999; revision accepted Sep. 14, 1999.

For correspondence or reprints contact: Matthias Bruehlmeier, MD, PET Program, Paul Scherrer Institute, CH-5232 Villigen, Switzerland.

**TABLE 1**
Comparison of Results of 6 WD Patients with Results of 16 Healthy Volunteers

| Subjects | Age (y) | Sex | Interval chelator therapy stopped before PET (d) | Iron uptake into brain: Ki (1/min) | Rate of iron clearance from plasma (1/min) | Cp in plasma (mg/L) |
|---|---|---|---|---|---|---|
| Patients | 23 | M | 5 | 10.90E-05 | 0.0137 | 15 |
| | 26 | M | 6 | 5.53E-05 | 0.0126 | 22 |
| | 39 | F | 21 | 6.87E-05 | 0.0095 | — |
| | 51 | M | 60 | 50.10E-05 | 0.0298 | 80 |
| | 42 | M | Chelator therapy during PET | 4.19E-05 | 0.0132 | 50 |
| | 28 | F | No chelator therapy before PET | 13.10E-05 | 0.0122 | 68 |
| Mean ± SEM | 36* | | | 15.12E-05 ± 7.13E-05 | 0.0152 ± 0.0030 | 47 ± 12 |
| Healthy volunteers | 65 | F | | 3.66E-05 | 0.0073 | |
| | 68 | F | | 3.34E-05 | 0.0067 | |
| | 64 | F | | 1.74E-05 | 0.0064 | |
| | 78 | F | | 3.54E-05 | 0.0109 | |
| | 42 | M | | 1.25E-05 | 0.0084 | |
| | 38 | M | | 4.33E-05 | 0.0080 | |
| | 45 | F | | 1.66E-05 | 0.0062 | |
| | 45 | F | | 3.17E-05 | 0.0093 | |
| | 60 | M | | 2.18E-05 | 0.0124 | |
| | 63 | F | | 2.99E-06 | 0.0063 | |
| | 62 | M | | 5.05E-06 | 0.0069 | |
| | 64 | M | | 4.86E-05 | 0.0125 | |
| | 52 | M | | 4.31E-05 | 0.0062 | |
| | 37 | F | | 3.03E-05 | 0.0068 | |
| | 58 | M | | 1.33E-05 | 0.0072 | |
| | 66 | F | | 3.35E-05 | 0.0078 | |
| Mean ± SEM | 57* | | | 2.66E-05 ± 0.35E-05 | 0.0081 ± 0.0005 | 150–600† |

*Mean age.
†Range of normal Cp levels in plasma of healthy volunteers.

### PET Data Acquisition

Each subject's head was aligned parallel to the orbitomeatal line and fixed in an individually molded thermoplastic head support. A dynamic series of PET images was obtained on a model 933/04-16 PET scanner (CTI/Siemens, Inc., Knoxville, TN) at the Paul Scherrer Institute. Seven planes with 8-mm thickness (also limiting transaxial resolution to 8 mm) were recorded simultaneously, yielding a total transaxial field of view of 56 mm. The gantry was positioned to image the brain from 10 to 66 mm above the orbitomeatal line, containing the upper half of the cerebellum, the whole temporal lobe, the lower part of the frontal lobe, the thalamus, and the basal ganglia. First, a 10-min transmission scan was obtained using a $^{68}$Ga ring source. Then, 15–18.5 MBq (0.4–0.5 mCi) $^{52}$Fe-citrate were infused intravenously during 3 min using a constant-volume infusion pump, and emission scans consisting of 18 frames within a total scan duration of 110 min were obtained simultaneously. Nineteen arterial blood samples were drawn from a catheter that was positioned in a radial artery. The radioactivities of whole blood and plasma were measured using a well counter. Radioactivity binding to the cellular blood fraction was determined separately by a repetitive centrifugation and washing procedure, yielding values of 1.5%–3% of whole-blood radioactivity. We used the measured plasma radioactivity as the input function for PET data modeling. To allow direct comparisons of plasma and tissue measurements, the well counter and the PET scanner were cross-calibrated after performing phantom experiments.

### Regions of Interest

$^{52}$Fe-citrate PET images are of low visual quality (Fig. 1) because of the low dose of radioactivity administered to subjects; this results in low-count images. Few anatomic landmarks in the brain are visualized by $^{52}$Fe-citrate PET. The leptomeninges, the basal cisterns including the pituitary area, and the choroid plexus show a relatively high tracer uptake, whereas the temporal bones are photon-deficient areas. The placement of regions of interest (ROIs) in the brain was based on identification and localization of these intracranial structures. High tracer uptake in the leptomeninges implicates a significant partial-volume effect in cortical ROIs. Thus, we placed ROIs (which were large to obtain a sufficient count statistic) in the frontal and occipital lobes with a considerable distance to the leptomeninges. This means, that the frontal and occipital ROIs represent a mixture of white and gray matter rather than cortex. Additionally, we placed ROIs around the basal ganglia (including thalamus, pallidum, and putamen and also white matter) and in the cerebellum. For each ROI, dynamic tissue data were obtained (time–activity curves during 110 min). All ROIs (frontal, occipital, basal ganglia, and cerebellum) were placed bilaterally on 2 separate planes, and the ROI values were then averaged for each brain region.

### Quantification of PET Data

PET tissue data and plasma radioactivity were used to calculate transport rates and the plasma distribution volume of $^{52}$Fe-citrate in the brain. We applied 2 different mathematic models to our data and

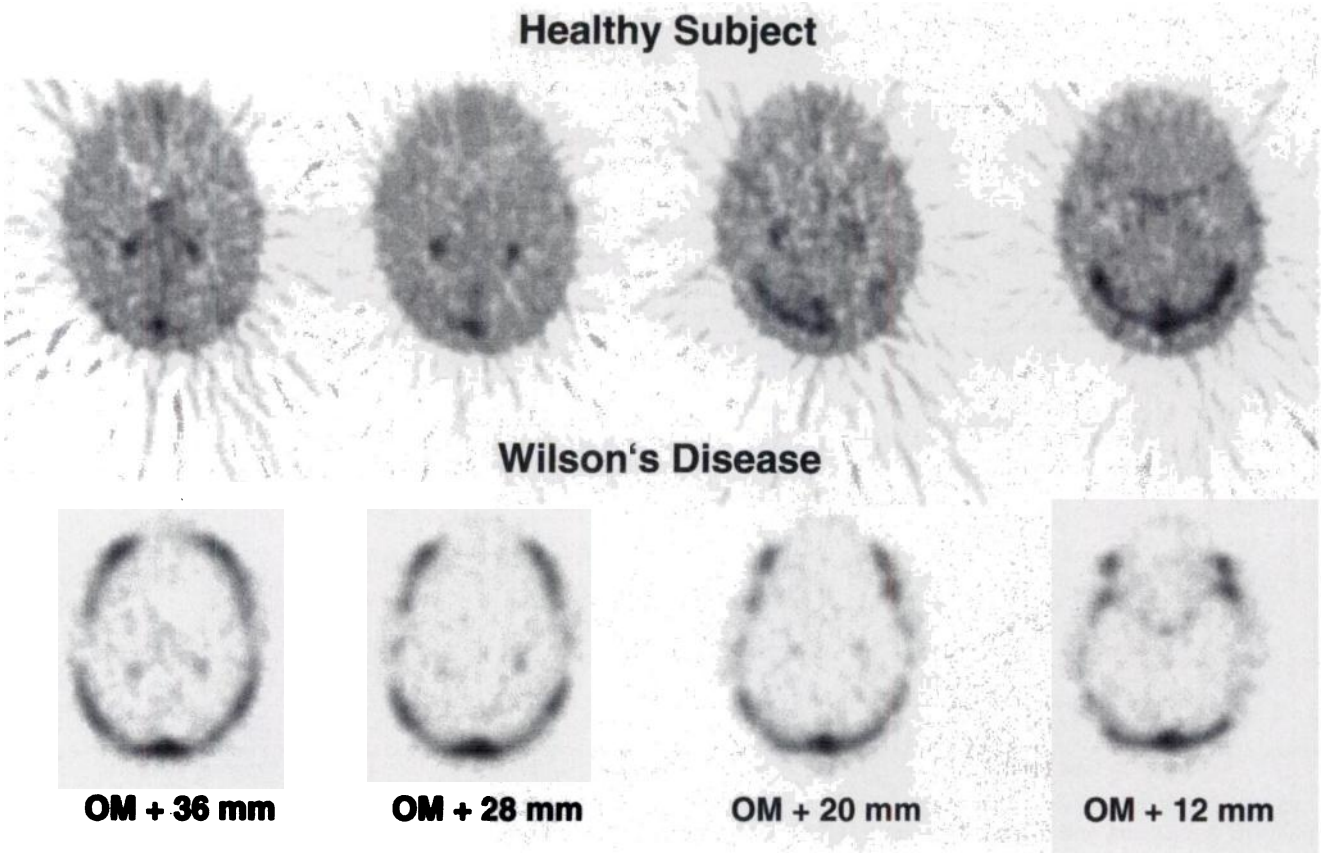


**FIGURE 1.** PET images of healthy volunteer (top) and male WD patient (51 y; bottom), which were obtained by adding time frames from 60 min until 110 min after injection. Images of both subjects are typical for each group: WD patients generally show higher tracer accumulation in leptomeninges and lower tracer uptake in choroid plexus than do healthy volunteers. Each image is normalized to its own maximum. OM + x mm = mean distance of transversal planes above orbitomeatal line.

compared the results of both methods by a Spearman's rank correlation analysis.

*Two-Tissue-Compartment Model.* Assuming tracer transport between plasma and 2 tissue compartments, this model describes the respective transport constants and the tracer distribution volume in plasma (rcpv, regional cerebral plasma volume; K1 and k2, transport constants from plasma to the first tissue compartment and vice versa; k3 and k4, transport constants from tissue compartment 1 to compartment 2 and vice versa). The biologic correlates for these parameters (e.g., active or passive diffusion, transcytosis, receptor binding, intracellular trapping, and so on) have to remain open at this point. We used a computer program that predicted tissue radioactivity on the basis of tracer concentration in plasma and kinetic parameters (i.e., rcpv, K1, k2, k3, and k4) until the predicted total tissue curve best fit the measured PET data (least-squares curve fitting). The quality of data fits was assessed by introducing an increasing number of parameters (1, rcpv alone; 2, rcpv and K1; 3, rcpv, K1, and k2; and so on). According to Hawkins et al. (*15*), the Akaike and Schwartz criteria were used to determine the minimal number of free parameters that were needed to sufficiently explain PET data.

*Multiple Time Graphic Plot.* The multiple time graphic plot (MTGP) (*16*) can be used to describe a net tracer influx (Ki) from blood into tissue. The amount of trapped tracer in tissue (at time tx after tracer injection) depends on the tracer concentration in plasma and on the time during which tissue was exposed to the respective tracer concentration. Tracer influx in tissue is reflected by a gradual increase of the ratio of tissue radioactivity to plasma radioactivity during the PET scan. To account for variable tracer concentration before tx, tx has to be transformed into the so-called exposure time (integral of tracer concentration in plasma from time 0 to tx, divided by the tracer concentration in plasma at tx (*16*)).

We applied the MTGP to our PET data because, during the scan time of 110 min, there was no measurable tracer efflux from the brain. Considering the fast initial changes of tracer concentration in plasma and the undesired influence of manganese, we plotted MTGP data points from 22.5 min (midtime of frame 9) after injection until the end of the scan at 110 min. Linear regression analysis allowed estimation of the distribution volume of $^{52}$Fe-citrate at time 0 ([Vd] initial ratio of brain radioactivity to plasma radioactivity as indicated by the intercept of the linear trend line through the MTGP data points on the y-axis) (Fig. 2). The slope of the trend line represents the rate constant Ki, which equals (K1 × k3)/(k2 + k3) of a 2-tissue-compartment model or K1 if k2 = 0. In the latter case, the model cannot discriminate between K1 and k3.

## RESULTS

The tracer concentration in brain was considerably lower than that in plasma (Fig. 2, left). When using a lower scale to plot brain radioactivity (Fig. 2, middle), the shape of the total tissue radioactivity curve resembled the plasma curve.

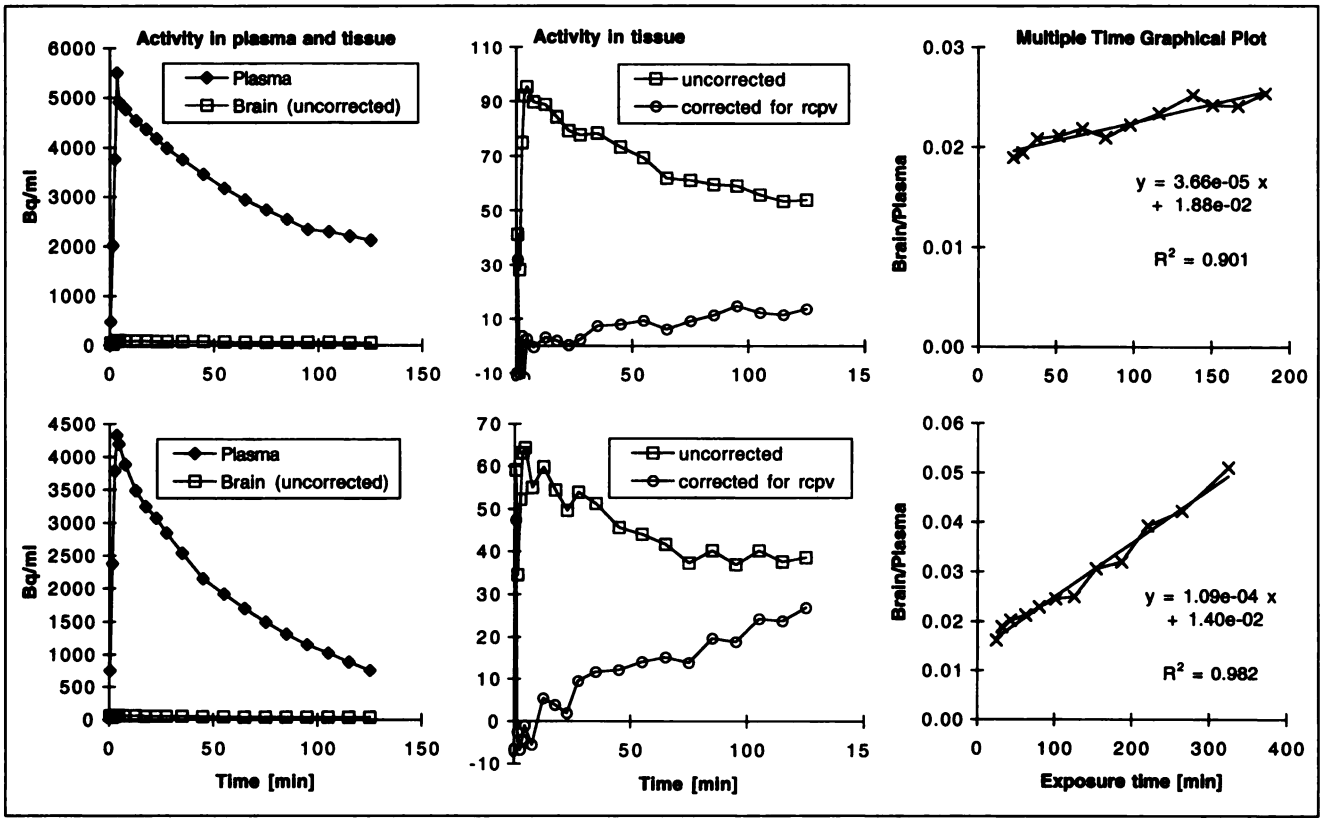


**FIGURE 2.** Tissue and plasma data and MTGPs of healthy volunteer shown in Figure 1 (top) and 23-y-old male WD patient (bottom). Latter graphs show higher iron uptake into brain tissue and faster disappearance of tracer iron from plasma.

Thus, one could suspect that the tissue curve represents solely the tracer distribution in the blood compartment. Therefore, we estimated rcpv for each ROI by averaging the ratio of brain radioactivity to plasma radioactivity during the first 27.5 min (neglecting tracer uptake into the brain during this time). The tissue time–activity curve (measured by PET) was then corrected for the expected intravascular signal by subtracting the ROI-specific rcpv multiplied by the plasma radioactivity at the respective time. This method revealed a slow, yet continuous, tracer uptake from blood into brain tissue (Fig. 2, middle, lower curves). This is also reflected by the linearity of the MTGP data points with a positive slope (Fig. 2, right).

To evaluate the quality of fitting the rcpv, K1, k2, k3, and k4 to PET data, we applied the Akaike and Schwartz criteria according to Hawkins et al. (*15*). Generally, we found these criteria to be lowest (i.e., optimal) when modeling PET data using only 2 free parameters (i.e., rcpv and K1). There was no improvement of data fitting by introducing further free parameters (k2, k3, and k4) in any subject. However, in 4 of 16 healthy volunteers, PET data could be explained by rcpv alone, and K1 could not be proven to be significantly different from zero ($P > 0.05$). Also, in 1 of 6 WD patients, K1 could not be proven to be different from zero ($P > 0.05$), although this patient's K1 was 0.00043 (in the upper range of a normal K1), indicating a significant error of the mean in estimating K1 in this patient. Another patient with a Ki clearly above the normal range had a normal K1 (Fig. 3A). Figure 3 also shows an unreasonable K1 = 0 in 1 healthy volunteer with a Ki that was significantly different from zero (open circle on the x-axis). A relatively low count statistic of our PET images may contribute to these discrepancies. Our impression was that the MTGP results (Ki) are more consistent than was data fitting to the 2-tissue-compartment model (considering outliers and error estimation of K1 and Ki). However, when examining all 22 subjects, there was a highly significant correlation between K1 and Ki ($P < 0.001$, Spearman's rank correlation analysis). Although this correlation was also found in 16 healthy volunteers ($P < 0.05$), the Spearman's rank correlation analysis failed to prove a significant correlation, Ki/K1, in the 6 WD patients alone ($P = 0.085$), most likely because of the K1 outliers.

However, both Ki and K1 were significantly ($P < 0.001$, Mann-Whitney test) higher in WD patients (Ki [mean ± SEM] = 15.1E-05 ± 7.13E-05 [1/min]) than in healthy volunteers (Ki = 2.66E-05 ± 0.351E-05 [1/min]) (Fig. 4). No correlation was found between Ki and each patient's Cp level in the plasma. In healthy volunteers and patients, no correlation was found between Ki and each subject's age or sex. Independence of Ki from age was important because the mean ages of the control group and the patient group differed considerably. As expected, rcpv correlated with Vd in healthy volunteers and in WD patients ($P < 0.001$, Spearman's rank correlation), but this correlation did not reach

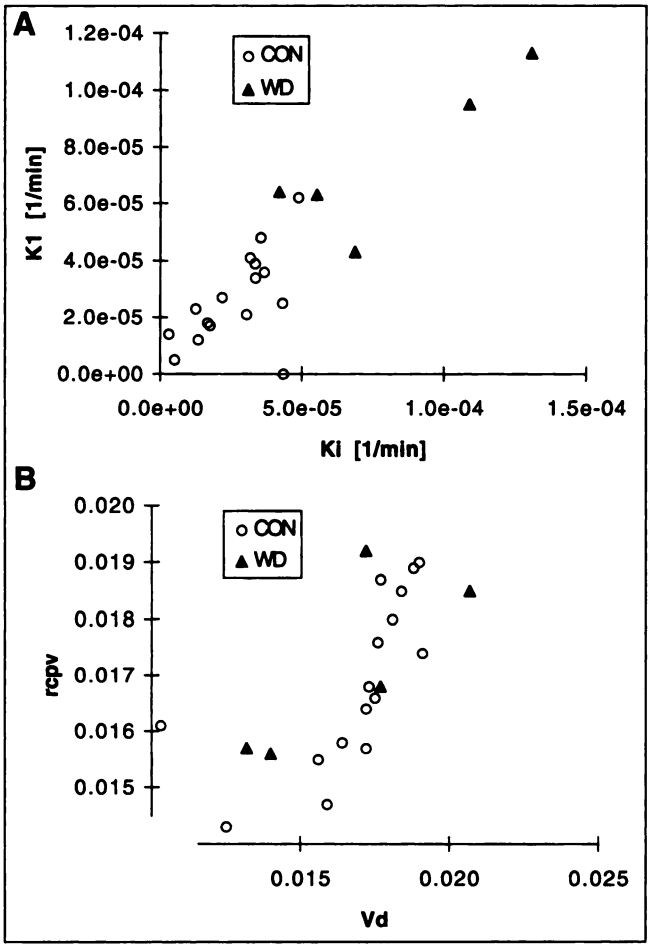


**FIGURE 3.** (A) Scatter plot of K1 versus Ki in WD patients and healthy volunteers (CON). For reasons of scaling, 1 WD patient (male, 51 y) with high Ki and K1 values is not included. (B) Scatter plot of rcpv versus Vd in both groups.

significance when examining 6 WD patients alone. There was no significant difference of rcpv or Vd between healthy volunteers and WD patients.

Figure 4 shows that differences of Ki between 4 brain regions are small in both groups. In WD patients, Ki is increased in all brain regions.

We plotted plasma activity of the $^{52}$Fe signal in patients and healthy volunteers on a semilogarithmic scale against time after injection (starting 5 min after injection). Data points followed a single linear trend, with the slope of this trend line denoting the rate of monoexponential tracer disappearance from plasma. This rate was significantly ($P <$ 0.002, Mann-Whitney test) higher in WD patients (mean ± SEM = 15.2E-03 ± 2.99E-03 [1/min]) than in healthy volunteers (8.08E-03 ± 0.53E-03 [1/min]). However, this difference was caused in part by an outlier (1 male WD patient, 51 y), which also had a very high Ki. For all other patients and all healthy volunteers, there was no correlation between Ki and the rate of tracer clearance from plasma (Fig. 5). This finding indicated that increased Ki values in WD patients were not associated with faster tracer clearance from plasma.

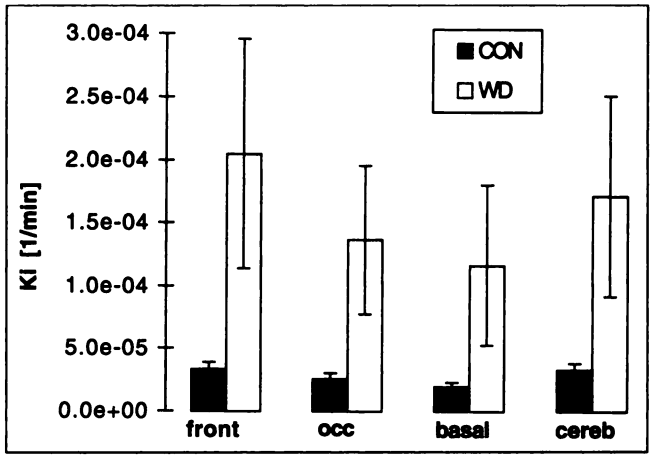


**FIGURE 4.** Ki values of different brain regions in 16 healthy volunteers (CON) and 6 WD patients (group averages ± SEM). Front = frontal; occ = occipital; basal = basal ganglia, thalamus, and central white matter; cereb = cerebellum.

## DISCUSSION

$^{52}$Fe-citrate PET provides a means to study the physiologic iron transport through the BBB into the brain. Both natural iron and $^{52}$Fe are almost completely bound to Tf in plasma. Because of its very low concentration in plasma, a trace amount of $^{52}$Fe does not significantly influence the saturation of Tf with iron nor does it compete with natural, nonradioactive iron about the brain entrance. There is no difference between natural iron and $^{52}$Fe in terms of its chemistry and behavior in vivo.

Our results show that the rate of iron uptake into the brains of WD patients is higher than that in healthy subjects, whereas the iron distribution in the cerebral plasma volume is the same in both groups. The first finding is surprising, considering that Cp deficiency is a common feature in WD patients. Cp plays an important role in the transmembranous

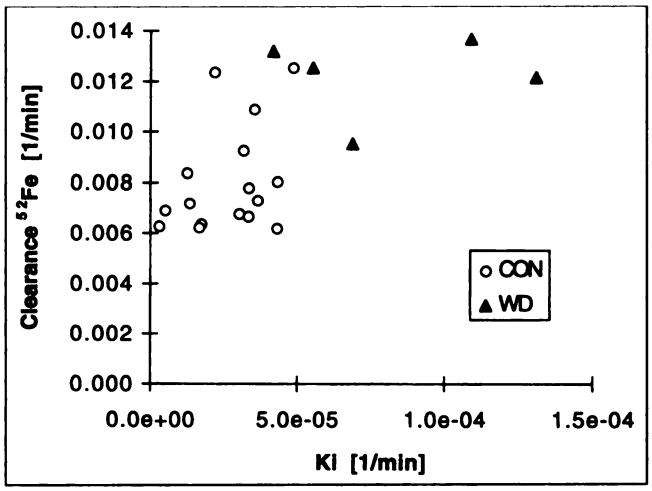


**FIGURE 5.** Rates of monoexponential plasma disappearance of $^{52}$Fe-citrate versus Ki in healthy volunteers (CON) and WD patients. For reasons of scaling, 1 WD patient (male, 51 y) with a high rate of tracer disappearance from plasma and high Ki is not included.

transport of iron. In a recent study, Mukhopadhyay et al. (*9*) reported a stimulating effect of Cp on the cellular iron uptake. On the other hand, Young et al. (*10*) reported that Cp facilitates the release of iron from HepG2 human liver cells in the presence of either extracellular apotransferrin or ferrotransferrin, especially under conditions of limited oxygen supply. Hereditary Cp deficiency in humans is associated with hemosiderosis of visceral organs and brain tissue (*11*), also suggesting a role of Cp in the release of iron from tissue. One might expect that Cp deficiency in WD patients would lead to a slower transport of iron through the BBB, depending on transcytosis of ferrotransferrin through the endothelium of brain capillaries. Of course, in vitro findings from cell cultures are not directly comparable with the brain iron transport in vivo. For example, brain tissue oxygenation could limit the oxidation of iron into its ferric transport form. Furthermore, cell cultures have no vascular barrier, and transmembranous iron transport in cell cultures does not necessarily depend on the Tf–Tf receptor (TfR) system (*9*), as is the case in the brain. However, it is unlikely that Cp deficiency accounts for the increased cerebral iron uptake in WD patients. The question arises whether the primary enzymatic defect in WD (deficiency of ATP7B) impairs the incorporation of copper into enzymes other than Cp. In Menkes' syndrome, another hereditary disorder of copper metabolism with a defective P-type adenosine triphosphatase (ATP7A) highly homologous to ATP7B, malfunctioning of the copper-containing cytochrome c oxidase has been recognized (*3*). Other copper-dependent enzymes play a role in mitochondrial energy metabolism—e.g., the cytochromes $a$ and $a_3$—which might be affected in WD. One could speculate whether a disturbance of respiratory enzymes (by a metabolic copper disorder) is partially compensated by upregulation of iron-dependent enzymes and therefore leads to a higher cellular need for iron.

Therapy with metal chelators is commonly used in WD patients. This could also possibly influence the iron uptake into the brain, either directly by interacting with tracer iron or indirectly by emptying metal stores in tissue. Also, the chelator desferrioxamine has been shown to increase the total cell receptors for ferrotransferrin in in vitro studies with K562 cells (*17*). However, in our patients, chelator therapy (e.g., triethylenetetramine dihydrochloride or D-penicillamine) was stopped several days or weeks before PET examination or was not established yet in all but 1 patient (42-y-old man). This latter patient was treated orally with D-penicillamine during the PET examination. Interestingly, this was the only patient with a Ki in the normal range of healthy volunteers; this finding possibly reflects the desired therapeutic mechanism of D-penicillamine with complexation and consequently lowered concentration of free plasma metal ions (iron and copper) available for uptake into the brain. Another patient (28-y-old woman), in whom WD had been diagnosed immediately before $^{52}$Fe-citrate PET and who had not yet been treated with chelators, showed an elevated brain iron uptake in the range of other WD patients. Furthermore, no correlation was found between Ki and the length of chelator therapy pause before PET. For these reasons, it is unlikely that the elevated brain iron uptake in WD can be explained by chelator therapy.

There are some limitations to our results and to $^{52}$Fe-citrate PET in general. First, and most important, $^{52}$Fe cannot be injected as a pure radionuclide. In a steady-state condition of nuclide decay, a solution of $^{52}$Fe always contains approximately 4% $^{52m}$Mn, which is also a positron emitter and therefore contributes to the time–activity curves measured by PET. This issue has been addressed in an animal model (*Macaca mullata* monkeys), where both pure manganese and a mixture of $^{52}$Fe and $^{52m}$Mn were injected (*18*). The transport rate of pure manganese into the monkey's brain was determined in the first step. The expected amount of manganese in the brain could be calculated by separate measurements of manganese and iron radioactivities in arterial blood by injecting both iron and manganese in the same animal for a second scan. This allowed correction of the measured (total) PET data for the manganese part, yielding pure iron transport data. Consequently, the kinetics of iron were calculated on the basis of the measured (total) and the corrected PET data. Calonder et al. (*18*) showed that, except for the first minutes after tracer injection, the influence of manganese on PET data could be neglected. This finding was explained mainly by the fast manganese disappearance from plasma after tracer administration and by a low brain uptake during scanning. The suggestion was made that the measured PET data (the signals of both iron and manganese) could be used as a valid basis for calculation of iron kinetics in this animal model. The question remains, however, if this is also valid for humans.

Second, the physiologic meaning of pharmacokinetic parameters in $^{52}$Fe-citrate PET has to be questioned. Quantitative PET measures the spatial and temporal characteristics of the tracer distribution in vivo to derive physiologically relevant variables. The tracer kinetic models used for that purpose are often simplified descriptions of the exact physiologic process under investigation. Little is known about the kinetics of iron in the brain. TfRs are densely localized on endothelial cells of brain capillaries (*19*); accordingly, binding capacity of $^{125}$I-Tf in cerebral microvessels (reflecting TfR density) has been found to be severalfold higher than in brain tissue (*20*). Ferrotransferrin crosses the BBB by receptor-mediated transcytosis (*21,22*). Because trace amounts of $^{52}$Fe rapidly and almost completely bind to plasma Tf in rhesus monkeys (*23*) and humans (*24*), we assume that transcytosis of the Tf–TfR complex will determine the tracer uptake into the brain after $^{52}$Fe-citrate administration. However, other transport mechanisms and further compartments beyond the BBB (e.g., an intracellular compartment) might also play a role.

Our results do not allow drawing a conclusion about the release of iron from the brain and the transport of iron within brain compartments. Statistically, we cannot prove k2, k3, and k4 to be different from zero (k2 = release of tissue iron

into blood; k3 and k4 = iron transport between brain tissue compartments). In other words, a 1-tissue-compartment model can explain our PET data and there is no benefit of introducing further tissue compartments into the model. It is important to recognize that this does not mean that k2, k3, and k4 = 0. Our data indicate that by means of $^{52}$Fe-citrate PET scanning over 2 h, it is impossible to measure k2, k3, and k4 in the brain. This finding may be attributed to a very low K1 (compared with K1 of other brain tracers), resulting in tracer concentrations in brain tissue that are in the range of only 1% of the plasma concentration, even at the very end of scanning (Fig. 2). Therefore, net tracer efflux resulting from k2 (even if it were as high as K1) would still be 100-fold lower than tracer influx. Limited count statistics of $^{52}$Fe-citrate PET images may additionally account for the fact that our PET data cannot determine an iron efflux from the brain. However, it is unlikely that k2 = 0 because this would lead to a fast overload of natural, nonradioactive iron of the brain.

## CONCLUSION

Our PET data show an abnormally increased iron influx into the brain of WD patients, which apparently coexists with (well-recognized) toxic copper uptake in liver and brain tissue. Our observation might explain neuropathologic findings of an increased iron deposition in many brain regions of WD patients. The cause of the involvement of iron in WD remains speculative. Cp deficiency or therapy with metal chelators is unlikely to explain these results.

## REFERENCES


1. Yarze JC, Martin P, Munoz SJ, Friedman LS. Wilson's disease: current status. *Am J Med.* 1992;92:643–654.
2. Brewer GJ, Yuzbasiyan-Gurkan V. Wilson disease. *Medicine (Baltimore).* 1992;71: 139–164.
3. Tumer Z, Horn N. Menkes disease: recent advances and new insights into copper metabolism. *Ann Med.* 1996;28:121–129.
4. Bowcock AM, Farrer LA, Cavalli-Sforza LL, et al. Mapping the Wilson disease locus to a cluster of linked polymorphic markers on chromosome 13. *Am J Hum Genet.* 1987;41:27–35.
5. Bowcock AM, Farrer LA, Hebert JM, et al. Eight closely linked loci place the Wilson disease locus within 13q14-q21. *Am J Hum Genet.* 1988;43:664–674.
6. Farrer LA, Bowcock AM, Hebert JM, et al. Predictive testing for Wilson's disease using tightly linked and flanking DNA markers. *Neurology.* 1991;41:992–999.
7. Yamaguchi Y, Heiny ME, Gitlin JD. Isolation and characterization of a human liver cDNA as a candidate gene for Wilson disease. *Biochem Biophys Res Commun.* 1993;197:271–277.
8. Bull PC, Thomas GR, Rommens JM, Forbes JR, Cox DW. The Wilson disease gene is a putative copper transporting P-type ATPase similar to the Menkes gene. *Nat Genet.* 1993;5:327–337.
9. Mukhopadhyay CK, Attieh ZK, Fox PL. Role of ceruloplasmin in cellular iron uptake. *Science.* 1998;279:714–717.
10. Young SP, Fahmy M, Golding S. Ceruloplasmin, transferrin and apotransferrin facilitate iron release from human liver cells. *FEBS Lett.* 1997;411:93–96.
11. Morita H, Ikeda S, Yamamoto K, et al. Hereditary ceruloplasmin deficiency with hemosiderosis: a clinicopathological study of a Japanese family. *Ann Neurol.* 1995;37:646–656.
12. Roeser HP, Lee GR, Nacht S, Cartwright GE. The role of ceruloplasmin in iron metabolism. *J Clin Invest.* 1970;49:2408–2417.
13. Smith-Jones P, Schwarzbach R, Weinreich R. The production of $^{52}$Fe by means of a medium energy proton accelerator. *Radiochim Acta.* 1990;50:33–39.
14. Blauenstein P, Pellikka R, Schubiger PA. Reinvestigation of a physiological eluate of the $^{52}$Fe/$^{52m}$Mn generator. *Appl Radiat Isot.* 1997;48:1097–1101.
15. Hawkins RA, Phelps ME, Huang SC. Effects of temporal sampling, glucose metabolic rates, and disruptions of the blood-brain barrier on the FDG model with and without a vascular compartment: studies in human brain tumors with PET. *J Cereb Blood Flow Metab.* 1986;6:170–183.
16. Patlak CS, Blasberg RG. Graphical evaluation of blood-to-brain transfer constants from multiple-time uptake data: generalizations. *J Cereb Blood Flow Metab.* 1985;5:584–590.
17. Mattia E, Rao K, Shapiro DS, Sussman HH, Klausner RD. Biosynthetic regulation of the human transferrin receptor by desferrioxamine in K562 cells. *J Biol Chem.* 1984;259:2689–2692.
18. Calonder C, Würtenberger PI, Maguire RP, Pellikka R, Leenders KL. Kinetic modeling of Fe-52/Mn-52m-citrate at the blood-brain barrier by positron emission tomography (PET). *J Neurochem.* 1999;73:2047–2055.
19. Jefferies WA, Brandon MR, Hunt SV, Williams AF, Gatter KC, Mason DY. Transferrin receptor on endothelium of brain capillaries. *Nature.* 1984;312:162–163.
20. Kalaria RN, Sromek SM, Grahovac I, Harik SI. Transferrin receptors of rat and human brain and cerebral microvessels and their status in Alzheimer's disease. *Brain Res.* 1992;585:87–93.
21. Fishman JB, Rubin JB, Handrahan JV, Connor JR, Fine RE. Receptor-mediated transcytosis of transferrin across the blood-brain barrier. *J Neurosci Res.* 1987;18:299–304.
22. Pardridge WM, Eisenberg J, Yang J. Human blood-brain barrier transferrin receptor. *Metabolism.* 1987;36:892–895.
23. Leenders KL, Antonini A, Schwarzbach R, et al. Blood to brain iron uptake in one rhesus monkey using [Fe-52]-citrate and positron emission tomography (PET): influence of haloperidol. *J Neural Transm Suppl.* 1994;43:123–132.
24. Leenders KL, Antonini A, Schwarzbach R, et al. Blood to brain iron transport in man using [Fe-52]-citrate and positron emission tomography (PET). In: Uemura K, Jones T, Lassen NA, Kanno I, eds. *Quantification of Brain Function: Tracer Kinetics and Image Analysis in Brain PET.* Amsterdam, The Netherlands: Elsevier; 1993:145–150.